Vehicle induced loads on pedestrian barriers

A. Sanz-Andres, A. Laveron, C. Baker, A. Quinn

This paper is a continuation of a previous one, Sanz-Andrés, Santiago-Prowald, Baker and Quinn (J. Wind Eng. Ind. Aerodyn. 91 (2003) 925) concerning the loads generated on a structural panel (traffic sign) by vehicle running along the road, although obviously, the results are also applicable to the effects of other moving vehicles such as trains. The structural panel was modelized as a large plate whose largest dimension is perpendicular to the vehicle motion direction. In this paper a similar approach is used to develop a mathematical model for the vehicle-induced load on pedestrian barriers, modelized as a large plate whose largest dimension is parallel to the vehicle motion direction. The purpose of the work is to develop a model simple enough to give analytical results, although with the physical phenomena correctly accounted for, such as to be able to explain, at least qualitatively, the main characteristics of the phenomenon, as observed in the experiments performed by Quinn et al. (J. Wind Eng. Ind. Aerodyn. 89 (2001) 831).

Actually, in spite of the model simplicity, results of the theoretical model show a reasonable good quantitative agreement with the experimental results. The aim of this and previous publications is to provide to the transport infrastructure community with some simple tools that can help to explain, and in some cases also to compute, the unsteady loading produced by moving vehicles on persons and installations placed close to the roads or tracks.

Nomenclature

b	barrier half-height (m)
c_F	net force coefficient
c_{F2S}	force coefficient in the case of two sources
$c_{F2S\mathrm{m}}$	maximum value of the force coefficient in the case of two sources
$c_{F\mathrm{m}}$	extreme value of the force coefficient c_F
c_p	pressure coefficient
$c_l(y)$	point force coefficient
c_N	dummy variable
c_s	configuration parameter
d	distance from the barrier to the body middle plane (m)
d_q	distance between sources (m)
$f(\tau)$	complex potential (m^2/s)
h_b	barrier distance to ground (m)
k	ratio of source intensities
p	static pressure (Pa)
t	time (s)
t_p	characteristic time of vehicle pass
t_v	viscous time scale
x	barrier section position considered (m)
x_0	source position in ground-fixed reference frame (m)
x', r	vehicle fixed reference system (m)
x, y, z	ground fixed reference system (m)
A_b	twice the vehicle cross-sectional area, body cross-sectional area far downstream (m^2)
B	sign half-span (m)
F	net force, per unit length (N/m)
L	characteristic length
N	symmetry of the flow, $N = 1$ two-dimensional, $N = 2$ axisymmetric three-dimensional flow
Q, Q_1, Q_2	volumetric source intensity (m^3/s)
Re	Reynolds number
T	dimensionless time
U_∞	vehicle speed (m/s)
V	velocity modulus (m/s)
V_∞	incident speed modulus (m/s)
$(V_\infty)_y$	projection of V_∞ along y
$(V_\infty)_{xz}$	projection of V_∞ in the plane xz
X_r	dimensionless relative coordinate
$X_{r\mathrm{m}}$	dimensionless relative position of the force extremes
θ	position across the barrier in trigonometric variable (rad)
ρ	fluid density (kg/m^3)
α	speed orientation angle (rad)

φ total velocity potential function (m^2/s)
φ_1 axial velocity potential function (m^2/s)
φ_2 cross-flow velocity potential function (m^2/s)
$\tau = X' + iY'$ complex variable (m)
ν kinematic viscosity (m^2/s)
subscript "ref" reference values
subscript "t" partial derivative with respect to time, $\partial/\partial t$ (s^{-1})

1. Introduction

In a previous paper (Sanz-Andrés, Santiago-Prowald, Baker and Quinn, SSBQ) [1] a mathematical model to predict the vehicle-induced loads on two-dimensional (2D) vertical traffic signs has been presented. In this case the largest dimension of the sign is taken as that normal to the vehicle direction of travel. In the case of a pedestrian barrier, although it shows a behaviour similar to the one predicted by the traffic sign model, this model is not fully applicable because the geometry involved can be considered in some sense as 2D in planes perpendicular to the largest barrier dimension, which is often placed parallel to the vehicle direction of travel. Therefore, the aim of this paper is to present a new model, developed following an approach similar to the one described in SSBQ and [3], which is applicable to the pedestrian barrier geometry, and to compare its results with the available experimental data. The idea is to develop a simple model which allows to obtain analytical solutions, and which can explain the time variation of the force. The results obtained from the model could help to understand the phenomenon involved, the influence of the parameters of the configuration, and in the future help to design new experiments in a more rational way.

Full-scale measurements of the load on pedestrian barriers induced by vehicle motion have been performed by Quinn et al. [2] and have been used here to establish comparison with the theoretical model results.

The assumptions considered in the approach are similar to those presented in SSBQ, and are summarized below:

(1) The flow generated by the vehicle motion is a potential flow, at least in the field influenced by the vehicle front. Emphasis is placed on the nose effect; thus the effect of the wake, being outside this restriction, can be safely neglected. There is not any intention to explain the effect of the vehicle end, dominated by the turbulent generation of the wake.

(2) The two-dimensional (2D) or three-dimensional (3D) potential flow generated by the vehicle motion is represented as that produced by a moving source, with intensity Q, which is determined by considering the vehicle cross-sectional area, $A_b/2$, and the vehicle speed, U_∞. The 2D or axisymmetric flow thus obtained represents the vehicle itself, as the upper half of a horizontal axisymmetric body. The

horizontal plane represents the ground. This model is crude but allows obtaining analytical solutions where the influence of the involved parameters can be easily described.

(3) The size of the pedestrian barrier (a plate) is much smaller than the vehicle cross-sectional area, and is far enough from the source so that the influence of the barrier on the flow generated by the source can be neglected. Based on this assumption the complete problem can be split into two simplified problems: (1) a uniform, steady, incident flow around the vehicle (without the barrier); and (2) a uniform, non-steady, incident flow around the barrier, whose both intensity and direction are time dependent. The uniform, non-steady flow is the speed generated at the barrier position by the moving source representing the vehicle. The load caused by the latter flow on the barrier is calculated using 2D strip theory at one section plane on the barrier as the simulated vehicles passes.

(4) The pressure field is determined by using the non-steady potential flow Bernoulli equation.

(5) No wake is developed behind the barrier at the first moments of the vehicle pass, as the vehicle pass is very quick, thus the primary forces on the barrier just at the first moments are a result of rapid acceleration of the fluid. As shown below, the wake is not developed at the first vehicle passage time interval. The characteristic time of vehicle pass is $t_p = L/U_\infty$ (L is a characteristic length and U_∞ is the vehicle speed). The viscous time scale needed to develop a boundary layer leading to the production of a wake behind the barrier, containing vortices, is of the order of $t_v = L^2/\nu$, where ν is the kinematic viscosity. Therefore, $t_p/t_v = \nu/(LU_\infty) = 1/\mathrm{Re}$, where Re is the Reynolds number which usually is $\mathrm{Re} \gg 1$. Therefore, the pass is so quick that there is not time enough for a wake to be developed on the flow behind the barrier.

2. Vehicle-induced velocity field

The geometry of the problem is shown in Fig. 1. The vehicle is represented (in a reference frame (x', r) fixed to the vehicle) by a source placed in an incoming steady, uniform flow of speed U_∞ aligned with the x'-axis (which is the direction of the vehicle motion). If the vehicle has a squared cross-section shape, the barrier is close to the vehicle, and the vehicle height is much larger than barrier height, the flow induced by the vehicle at the barrier position is nearly 2D, as generated by an infinitely tall vehicle. Therefore, in these conditions the vehicle shape can be considered to be generated by a vertical source line (a 2D source, identified by $N = 1$ in the formulation). If the barrier is far enough away, the flow produced by the vehicle at the barrier position can be considered as axisymmetric and, therefore, the vehicle effect could be generated by a 3D source ($N = 2$). In the second case one could consider the situation to be analogous to the far field behaviour of the inner field in a slender body problem: in the case of a non-axisymmetric body the flow field close to the slender body is non-axisymmetric (unless the body is axisymmetric) and becomes axisymmetric as the distance from the body increases. In the context of the

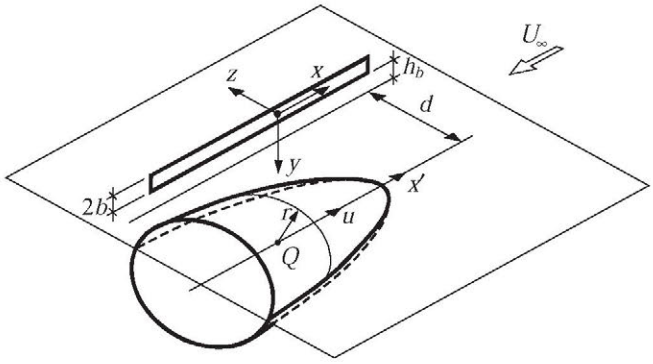

Fig. 1. Sketch of the configuration considered. (r, x') vehicle fixed reference system. (x, y, z) ground fixed reference system. d, distance from the vehicle path to the barrier location. Q, source intensity. h_b, distance from barrier to ground. $2b$, sign height. The axisymmetric case is represented.

slender body aerodynamics theory, the transformation of a non-axysimmetric field in an axysimmetric one as the distance from the body increases is known as the Oswatistch–Keune principle [4].

Therefore, the 2D and 3D solutions can be considered as asymptotic cases of a general configuration: if the barrier is close to the vehicle, the 2D flow should be considered, and the 3D flow applies at larger distances.

The pedestrian barrier, $2b$ high, is close to the ground (height h_b) in such a way that $2b \ll h_b$. The velocity V_∞ induced by the moving source in a barrier section x, and the speed orientation α, are given by (SSBQ)

$$V_\infty = \frac{Q}{2\pi N} \frac{1}{[(x - x_0)^2 + d^2]^{N/2}}, \tag{1}$$

$$\sin \alpha = \frac{d}{[(x - x_0)^2 + d^2]^{1/2}}, \tag{2}$$

where $N = 1, 2$ holds for 2D and 3D fields, respectively. d is the distance from the barrier to the body middle plane. x_0 is the source position in ground-fixed reference frame, $x_0 = U_\infty t$. V_∞ and α are functions of time through the dependence on x_0. The source intensity, Q, is determined by flow mass conservation considerations evaluating the mass flux through the body cross-sectional area far downstream, A_b, where incident flow speed intensity U_∞ is recovered

$$Q = U_\infty A_b. \tag{3}$$

Obviously, the evaluation and the dimensions of A_b in 2D and 3D cases is different. In the 2D case A_b (m) is the area of the unit length (just the vehicle width). In the 3D case the A_b dimension is (m^2).

3. Flow around a barrier section

As shown in Fig. 2, the flow impinging on each barrier section, x, has a different intensity $V_\infty(x - x_0)$, and direction, $\alpha(x - x_0)$, depending on the distance from the source position, x_0, to the section x considered. Close to the barrier, at a distance of the order of $b \ll d$, each section can be considered as a plate, $2b$ wide in the y direction, around which an almost 2D flow is established taking into account that the speed variation along x direction (with characteristic length d) is much smaller than speed variation along y direction (with characteristic length $b \ll d$), so that slender wing and body theory concepts can be applied to study this problem.

Let us split the problem shown in Fig. 2 in two simpler ones, by taking into account that the incident speed V_∞ can be considered as the sum of two components, one normal to the barrier (along z-axis) $V_\infty \sin\alpha$, and the other one parallel to the barrier (along x-axis) $V_\infty \cos\alpha$, as shown in Fig. 3. Each one of the two components leads to the so-called cross-flow problem and axial problem, respectively.

The barrier perturbs the normal impinging component, while the parallel component is not affected. The axial problem solution (Fig. 3b) in terms of the velocity potential function is

$$\varphi_1(x) = V_\infty x \cos\alpha. \tag{4}$$

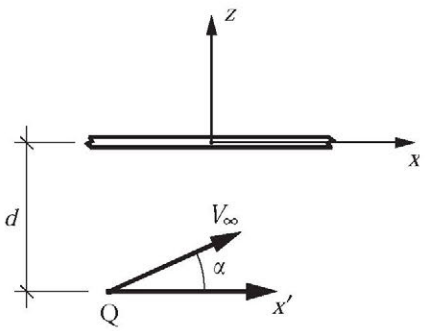

Fig. 2. Model of the flow impinging the barrier, generated by the vehicle V_∞, flow speed at the barrier position generated by the source Q. α, flow direction. x', body fixed reference system. d, distance from the vehicle path to the barrier location. (x, z), ground fixed reference system.

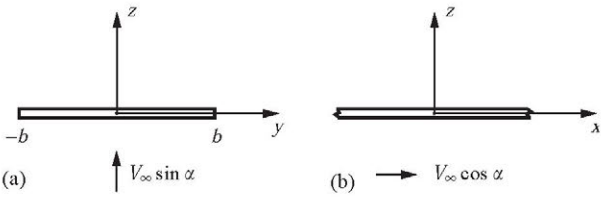

Fig. 3. Model of the flow. (a) Normal flow problem. (b) Axial flow problem.

The solution of the cross-flow problem is (as shown in SSBQ) based in the 2D flow complex potential solution

$$\varphi_2(y,z) = \mathrm{Re}\left[-\mathrm{i}V_\infty \sin\alpha\sqrt{\tau^2 - b^2}\right], \tag{5}$$

where $\tau = y + \mathrm{i}z$ is the complex variable in the (y,z) plane. Re is the real part.

This solution implies that the flow does not separate at the top edge of the barrier, in the case of an steady flow. However, it is difficult to say that the flow separates in the case of an unsteady, impulsive flow as justified in assumption (5). In addition to that, it can be shown that the speed produced by the pass of the vehicle is quite small. The main cause of the load is the change in the velocity potential, φ_t. To clarify whether the flow separation appears, dedicated experiments should be performed. In any case, the consideration of a separate flow would not change the main result of the work, which is the shape of the time variation of the force with time, and only would change the quantitative value. Note that the present problem is similar to the calculation of the added mass of the barrier and the consideration of the separated flow would just imply a change in the value of the added mass.

The total velocity potential function is

$$\varphi(x,y,z) = \varphi_1(x) + \varphi_2(y,z) = V_\infty\left[x\cos\alpha + \mathrm{Re}\left(-\mathrm{i}\sin\alpha\sqrt{\tau^2 - b^2}\right)\right]. \tag{6}$$

The pressure field, p, is obtained from the Bernoulli equation for non-steady potential flow

$$p + \tfrac{1}{2}\rho V^2 + \rho\varphi_t = p_{\mathrm{ref}} + \tfrac{1}{2}\rho V_{\mathrm{ref}}^2 + \rho\varphi_{\mathrm{ref}\,t}, \tag{7}$$

where the subscript "ref" indicates reference magnitudes. ρ is the fluid density. The speed and velocity potential function are zero far from the barrier, where the pressure is p_∞. Taking these values as the reference values, from (7) one obtains

$$p - p_\infty = -\tfrac{1}{2}\rho V^2 - \rho\varphi_t. \tag{8}$$

The pressure coefficient, c_p is given by

$$c_p = \frac{p - p_\infty}{\frac{1}{2}\rho U_\infty^2} = -\left(\frac{V}{U_\infty}\right)^2 - \frac{2\varphi_t}{U_\infty^2}. \tag{9}$$

The velocity and the potential function distributions on the plate are given by

$$\varphi(y) = V_\infty(x\cos\alpha \pm b\sin\alpha\sin\theta), \tag{10a}$$

$$V^2 = \varphi_x^2 + \varphi_y^2, \tag{10b}$$

where the + (−) sign applies for the surface away from the source, $z = 0^+$ (towards the source, $z = 0^-$) surface, and a more convenient variable has been used

$$y = b\cos\theta. \tag{11}$$

The point force coefficient, $c_l(y)$ is defined as the dimensionless pressure jump across the plate

$$c_l(y) = c_p(y, z = 0^-) - c_p(y, z = 0^+), \tag{12}$$

and therefore the dynamic pressure term V^2 and those of the terms in $\varphi(y)$ that are the same at both sides of the barrier do not contribute to the point force (remember that V^2 is the same in both faces). By using (9)–(12), the point force coefficient $c_l(y)$ is obtained

$$c_l(y) = \frac{4b}{U_\infty^2} \sin\theta \frac{\partial}{\partial t}(V_\infty \sin\alpha). \tag{13}$$

The force coefficient c_F of a barrier section is

$$c_F = \frac{F}{\frac{1}{2}\rho U_\infty^2 (2b)} = \int_{-b}^{b} c_l(y) \frac{\mathrm{d}y}{2b} = \frac{\pi b}{U_\infty^2} \frac{\partial}{\partial t}(V_\infty \sin\alpha), \tag{14}$$

where F is the net force, per unit length. The derivative term can be deduced from (1) and (2) to give

$$c_F(X_r) = \frac{N+1}{2N} \frac{bA_b}{d^{N+1}} \frac{X_r}{(X_r^2+1)^{(N+3)/2}} = \frac{N+1}{2N} c_s(N) \frac{X_r}{(X_r^2+1)^{(N+3)/2}}, \tag{15}$$

where use has been made of definition (3) of $Q = A_b U_\infty$. The dimensionless relative coordinate X_r is defined as

$$X_r = \frac{x - x_0}{d} = \frac{x - U_\infty t}{d} = X - T, \tag{16}$$

and the configuration parameter $c_s(N)$ is defined as

$$c_s(N) = \frac{bA_b}{d^{N+1}}.$$

$c_F(X_r)$ is shown in Fig. 4 for the 2D and 3D fluid configurations.

In expression (15) three dimensionless factors appear:

- The first factor $(N+1)/(2N)$ appears as a consequence of the different flows considered (2D or 3D).
- The second factor expresses the influence of the geometrical parameters of the configuration, the plate half-span b, the vehicle cross-sectional area A_b and the distance from the barrier to the vehicle trajectory d (in which the type of flow considered appears through the $N+1$ exponent).
- The third factor contains the space or time dependence. For instance, when $t = 0$ then $X_r = X = x/d$ and (15) gives the space-dependence $c_F(X)$ when the source passes at the origin of x-, y-, z-axis (or, that is the same, relative to the source instantaneous position). If a given point is considered, for instance $X = 0$, then the time variation $c_F(T)$ is obtained because $X_r = -U_\infty t/d = -T$, where T is the usual dimensionless time.

$c_F(X) = c_F(X, T = 0)$ is the instantaneous force distribution along the barrier (when the distance X is measured from the instantaneous source position) and $c_F(T) = c_F(X = 0, T)$ is the time variation at a given point. Both expressions are related as follows:

$$c_F(X_r) = c_F(X, t = 0) = c_F(X = 0, -T) = -c_F(X = 0, T).$$

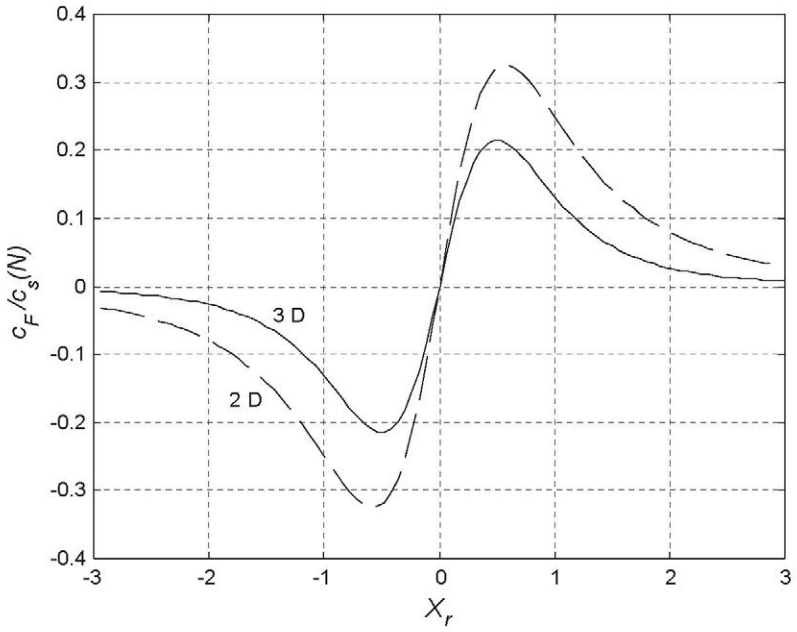

Fig. 4. Variation of the section force coefficient, c_F, with the dimensionless relative coordinate, X_r. $c_s(N)$ is the configuration parameter. $c_F > 0$ means force pushing out of the road.

As $c_F(X_r)$ is antisymmetric with regard $X_r = 0$, $c_F(X)$ and $c_F(T)$ are also antisymmetric.

The force distribution along the barrier shown in Fig. 4 and given by (15) can be shown as a force wave that is carried by the source along the barrier (if the barrier were of infinite length). The force experienced by the barrier is positive (directed outwards) as the vehicle is approaching and it suddenly changes to negative (directed towards the vehicle) as the vehicle pass by the barrier.

The force considered is mainly due to the front fraction of the vehicle. It should be recalled that the source model mainly represents an infinitely long vehicle, and therefore there is not a second pressure pulse associated to the pass of the vehicle rear portion.

The front portion effect on traffic signs is explained theoretically in [1] of the paper and experimentally shown in [5]: there is a clear pressure pulse associated to the nose pass, and other pulse associated to the rear portion of the vehicle (where the wake of the vehicle begins).

The reason for this separation of effects is the linear character of Eqs. (13) and (14), which give the force on the barrier. It is also shown in [1] that the model predicts the force even in a quantitative way in the case of an "streamlined" body, where the front and rear pulses can be clearly observed (Fig. 8 in [1]).

The positions ($X_r = X_{rm}$) of the force extremes $c_F(X_{rm}) = c_{Fm}$ are given by

$$X_{rm} = \pm\frac{1}{\sqrt{N+2}}, \tag{17}$$

and therefore, depending on the consideration given to the type of flow generated by the moving body at the barrier (2D or 3D) the extreme positions X_{rm} are closer to the source position. For $N = 1$, $X_{rm} = \pm 1/\sqrt{3}$ and for $N = 2$, $X_{rm} = \pm 1/2$.

The extreme values c_{Fm} are

$$c_{Fm} = \pm c_N(N)c_s(N), \tag{18}$$

where

$$c_N(N) = \frac{N+1}{2N(N+2)^{1/2}}\left(\frac{N+2}{N+3}\right)^{(N+3)/2} \tag{19}$$

and

$$c_N(1) = \frac{1}{\sqrt{3}}\left(\frac{3}{4}\right)^2 \simeq 0.325,$$

$$c_N(2) = \frac{3}{8}\left(\frac{4}{5}\right)^{5/2} \simeq 0.215,$$

which shows that 2D configurations produce larger forces than 3D flows.

4. The effect of the distance of the barrier to the ground

As the barrier is not flush with the ground, the image of the barrier should be included. Let us consider the effect of the barriers in its image, which is the same as the effect of the image on the barrier.

The asymptotic behaviour of the cross-flow problem solution (5) is that of a doublet of intensity $(b^2/2)V_\infty \sin\alpha$ and directed normal to the plate (along z-axis) (see Fig. 3a). The influence of this doublet on the image of the barrier (which is placed at $y = 2h_b + b$, $z = 0$) is limited to the speed normal to the plate, φ_{2z}

$$\varphi_{2z}(2h_b + b, 0) = \frac{1}{2}V_\infty \sin\alpha \frac{b^2}{(2h_b + b)^2} \simeq \frac{1}{2}V_\infty \sin\alpha\left(\frac{b}{2h_b}\right)^2,$$

because the effect on both the velocity potential function and speed component parallel to the barrier are zero:

$$\varphi_2(2h_b + b, 0) = 0,$$

$$\varphi_{2y}(2h_b + b, 0) = 0.$$

The relative change in normal speed in one barrier due to its image is therefore

$$\frac{\varphi_{2z}(2h_b + b, 0)}{V_\infty \sin\alpha} \simeq \frac{1}{2}\left(\frac{b}{2h_b}\right)^2 \simeq 1.3 \times 10^{-3}$$

when $b \cong 0.1 h_b$, which is a negligible effect as far as the global accuracy of the model is considered.

Other effect associated to the distance of the barrier to the ground is that the speed generated by the source at the barrier position is not really V_∞ as given by (1). In fact, the projections of V_∞ should be considered. V_∞ projected along y is given by

$$(V_\infty)_y \cong V_\infty \frac{h_b}{d}$$

and in the plane xz is

$$(V_\infty)_{xz} \simeq V_\infty \left[1 - \frac{1}{2}\left(\frac{h_b}{d}\right)^2\right],$$

if

$$\frac{h_b}{d} \ll 1, \quad h_b \gg 2b.$$

The component $(V_\infty)_y$ is not perturbed by the barrier (it just sweeps the barrier) and it is the same on both faces of the barrier; therefore there is not need to take it into account. Concerning $(V_\infty)_{xz}$, the error in considering just V_∞ is limited to an amount

$$\frac{1}{2}\left(\frac{h_b}{d}\right)^2.$$

5. The effect of the barrier on the moving vehicle

To evaluate the effect of the barrier on the moving vehicle, the far field due to the barrier perturbation should be analysed. From expression (5), in the limit $\tau \to \infty$ one obtains the asymptotic behaviour of the complex potential far from the barrier

$$f(\tau) \simeq -\mathrm{i} V_\infty \sin\alpha\tau + \mathrm{i} V_\infty \sin\alpha \frac{b^2}{2\tau}.$$

The first term represents the normal component of the impinging flow. The second term represents a doublet; therefore the barrier is seen as a doublet in the barrier far field. The doublet associated velocity field is (in modulus) $V_\infty \sin\alpha b^2/(2|\tau|^2)$. It means that at a distance four times the half-height b the speed experienced due to the barrier is 1/32 of the normal component of the speed impinging on the barrier, $V_\infty \sin\alpha$. This result supports assumption (3) in Section 1.

6. Comparison between theoretical and experimental results

The comparison between theoretical and experimental results of Fig. 8 in [2] is shown in Fig. 5. The values of the experimental configuration parameters considered are as follows: $A_b = 15\ \mathrm{m}^2$, $2b = 0.155$ m, $d = 3$ m (1.5 m of separation of the

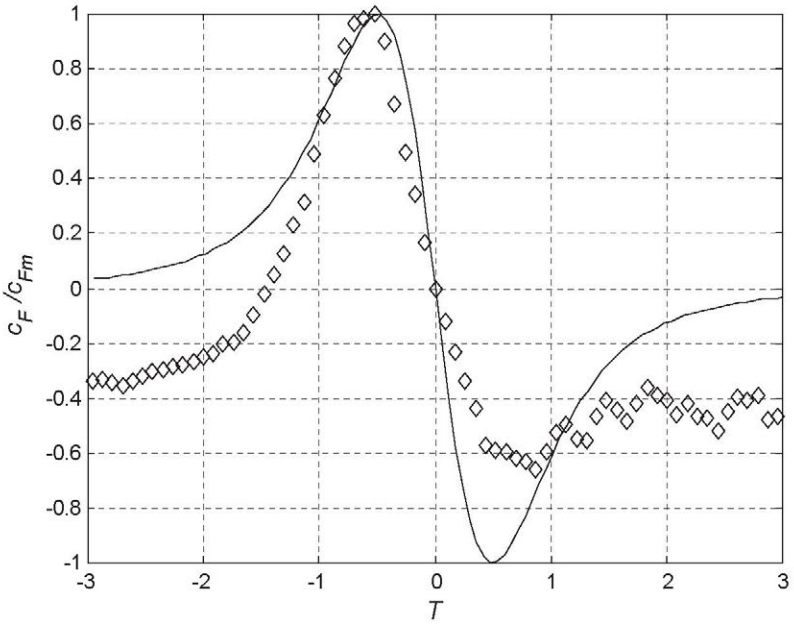

Fig. 5. Variation of the section force coefficient, c_F, with the dimensionless time, T. $c_F > 0$ means force pushing out of the road. c_{Fm} is the maximum value of the force coefficient. Solid line: theoretical model for 3D configuration. Diamonds: experimental results of Quinn et al. [2, Fig. 8] for a pedestrian barrier parallel to the road, by using $c_{Fm} = 0.015$.

barrier from the vehicle side plus 1.5 m distance from the vehicle middle plane to the vehicle side). The distance d chosen allows a good matching of the peaks position, and is considered an estimated mean value due to the difficulty of determining the distance in the experimental configuration (in fact we are dealing with normal traffic in a road, which shows fluctuations on vehicle speed, shapes, sizes and distances to the barrier).

The 3D model is arbitrarily chosen as the results of both theoretical models are qualitatively similar, and there is no aim for quantitative matching (in such a case a more detailed model of the vehicle should be employed).

By using the values of the experimental configuration parameters above mentioned, the theoretical force coefficient maximum value obtained is $c_{Fm} = 0.010$ (in the 3D configuration) which is close to the experimental value $c_{Fm} = 0.015$, although there is no claim for a quantitative agreement because of both the crudeness of the model and the election of the values of the parameters, which involved some degree of arbitrariness, as already mentioned.

The main feature of the comparison is that the shape of both curves (experimental and theoretical results) is quite similar, although there exists a significant difference: while in the theoretical model the asymptote is $c_F = 0$, in the experimental results the asymptotic value is $c_F \cong 0.4 c_{Fm}$ when $T \to +\infty$ or $T \to -\infty$. This asymptote could

be due to a permanent force acting on the sign, possibly due to the mounting of the barrier on the load cells not being exactly levelled when on the roadside, and then there might be an offset due to a component of the gravitational force. Other reason could be the cumulative effect of the wake. To clarify this phenomenon, dedicated additional experiments should be performed, once the potential effects are explained.

Just as an example to show the influence of the vehicle nose curvature, let us consider a fluid configuration generated by two singularities, one source with intensity $Q_1 = kQ$, and one sink of intensity $Q_2 = -(k-1)Q$, placed a distance d_q behind Q_1. In order to preserve the vehicle cross-sectional area the following condition holds:

$$Q_1 + Q_2 = Q.$$

The force coefficient in this case is given by the following expression:

$$c_{F2S}(T) = [c_F(T) + c_F(T + \Delta T)],$$

where $\Delta T = d_q/U_\infty$. The results obtained for $k = 2.5$ and $d_q = 0.4d$ are shown in Fig. 6, together with the experimental data of Quinn et al. [2, Fig. 8] It is shown the effect of the rupture of antisymmetry of the theoretical results and the enhanced matching between experimental data and theoretical results.

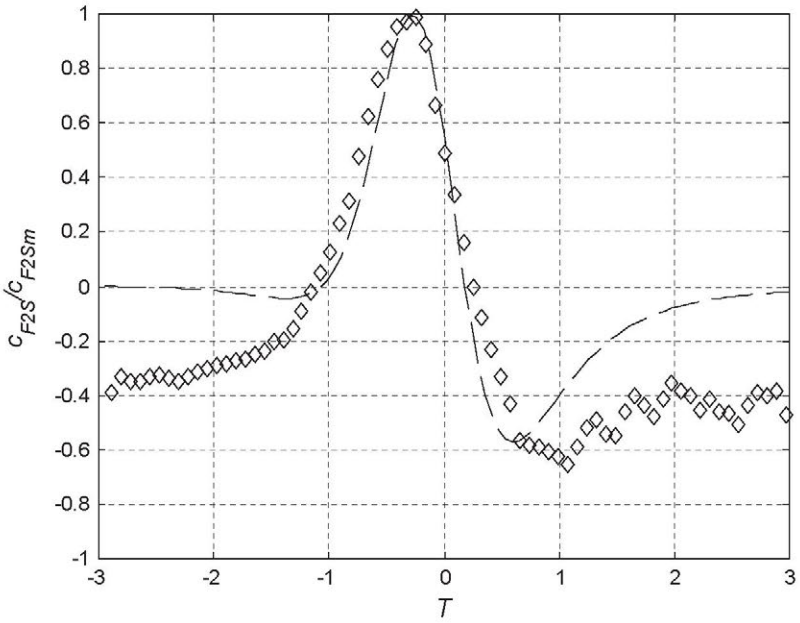

Fig. 6. Variation with the dimensionless time, T, of the section force coefficient c_{F2S} generated by a source and a sink. $c_{F2S} > 0$ means force pushing out of the road. c_{F2Sm} is the maximum value of the force coefficient. Solid line: theoretical model for 3D configuration. Diamonds: experimental results of Quinn et al. [2, Fig. 8] for a pedestrian barrier parallel to the road, by using $c_{Fm} = 0.015$. The experimental data are shifted in time an amount of 0.25.

7. Conclusions

These results are similar to that obtained by SSBQ concerning the traffic signs for the parallel configuration, taking always the smaller dimension as the half-span (B in traffic sign and b in pedestrian barriers) so care should be taken when the force is made dimensionless and when computing c_F.

The test results are in better agreement with experimental data when $T<0$ (before passing the source), as the antisymmetric behaviour with regard to $T = 0$ is not clear in the experimental results. This could be due to the strong simplification of the vehicle shape considered, just a single source. If an appropriated source distribution were taken into account (needed to increase the bluntness of the vehicle nose) then a tendency closer to the one experimentally observed would be obtained. However, some more experiments should be done in order to ascertain that when the vehicle is not close to the sign the value of the force coefficient is not zero.

The presented model is based on the existence of a potential flow. The applicability of the results are therefore limited by this circumstance. In order to obtain quantitatively significant results a more detailed (and with a broader application range) model should be developed, which takes into account turbulent effects such as the vehicle slipstream and wake, especially when considering the pressure field in the region affected.

[1] A. Sanz-Andrés, J. Santiago-Prowald, C. Baker, A. Quinn, Vehicle induced loads on traffic sign panels, J. Wind Eng. Ind. Aerodyn. 91 (2003) 925–942.

[2] A.D. Quinn, C.J. Baker, N.G. Wright, Wind and vehicle induced forces on flat plates. Part 2: Vehicle induced force, J. Wind Eng. Ind. Aerodyn. 89 (2001) 831–847.

[3] A. Sanz-Andrés, J. Santiago-Prowald, Train-induced pressure on pedestrians, J. Wind Eng. Ind. Aerodyn. 90 (2002) 1007–1015.

[4] H. Ashley, M. Landahl, Aerodynamics of Wings and Bodies, Dover, New York, 1985, p. 112.

[5] P.M. Cali, E.E. Covert, Experimental measurements of loads on an overhead highway sign structure by vehicle-induced gusts, J. Wind Eng. Ind. Aerodyn. 84 (2000) 87–100.